We are IntechOpen,
the world's leading publisher of
Open Access books
Built by scientists, for scientists

4,800
Open access books available

122,000
International authors and editors

135M
Downloads

Our authors are among the

154
Countries delivered to

TOP 1%
most cited scientists

12.2%
Contributors from top 500 universities

Interested in publishing with us?
Contact book.department@intechopen.com

Numbers displayed above are based on latest data collected.
For more information visit www.intechopen.com

Dielectrophoresis-Assisted Pathogen Detection on Vertically Aligned Carbon Nanofibers Arrays in a Microfluidic Device

Foram Ranjeet Madiyar, Omer Farooq and Jun Li

Additional information is available at the end of the chapter

Abstract

In this chapter, we focus on utilizing nanoelectrode arrays fabricated with vertically carbon nanofibers (VACNFs) for pathogen detection based on a "point-and-lid" dielectrophoretic device in a microfluidic channel. This technique is utilized to concentrate particles from the bulk flow and detect pathogens based on fluorescence, surface-enhanced Raman spectroscopy (SERS) and impedance measurements. The advantage of VACNFs is their ultrasmall diameter (~100 nm) and the high aspect ratio (50:1). When coupled with a macroscopic indium tin oxide (ITO) electrode, it produces a large electric field gradient ($\nabla E^2 = \sim 10^{19} - 10^{20}$ V^2 m^{-3}) which is harnessed for pathogen detection based on dielectrophoresis. Several noninfectious pathogens including bacteria *Escherichia coli* DHα5, inactivated vaccinia virus (species: *Copenhagen strain*, *VC-2*), and *Bacteriophage* T4r were utilized as model species to study the size effect and kinetics of dielectrophoretic capture in this study. The comparable size of the nanoelectrode produced strong interaction with virus particles, generating striking lightning capture patterns and high detection sensitivity. The dielectrophoretic capture at the nanoelectrode arrays is successfully integrated with a portable Raman probe as a microfluidic chip for ultrasensitive detection of bacteria *E. coli* DHα5 using SERS-tagged gold nanoparticles co-functionalized with specific antibodies.

Keywords: dielectrophoresis, pathogen detection, vertically aligned carbon nanofibers (VACNFs), nanoelectrode array (NEA), indium tin oxide (ITO), microfluidic device, electroporation, plaque-forming units (pfu), bacteria *E. coli* Dhα5, *Bacteriophage* T4r, vaccinia virus, iron-oxide gold nanoovals (IO-Au NOVs), surface-enhanced Raman spectroscopy (SERS), impedance, fluorescence

1. Introduction

The need for rapid and reliable pathogen monitoring and detection is imperative in the food industry, biodefense, drug discovery, animal healthcare, clinical diagnosis, water, and environmental quality control. Among these, the food industry is the area where most attention has been focused on due to public health implications. In 2015, the World Health Organization (WHO) estimated that 77 million people every year fall victim to contaminated food and about 9000 deaths annually. The WHO has identified 31 agents of foodborne diseases including bacteria, virus, parasites, toxins, and chemicals, among which 95% are caused by *Norovirus*, *Campylobacter*, *Escherichia coli*, and non-typhoidal *Salmonella* [1]. In recent years, there have been considerable efforts to develop devices and methods for capturing pathogens in fluids such as blood, food matrices, soil, bodily fluids, and water for rapid detection.

The conventional pathogen identification methods are standard microbiological techniques and involve necessary steps such as preenrichment, selective enrichment, biochemical screening, and serological confirmation [2]. The traditional methods take up to 72 h to obtain confirmed results which are based on the morphological evaluation, culture growth in various media under various conditions, and enumerating colonies of the bacteria [3, 4]. However, the development of polymerase chain reaction (PCR)-based molecular analysis techniques [5–7], the conventional biochemical methods such as enzyme-linked immunosorbent assays (ELISAs), and blot assays have led scientists to target genes, proteins, and carbohydrate moieties instead of the whole microorganisms [8] to obtain molecular fingerprints of the pathogens. These techniques despite being highly sensitive and selective require experienced personnel, expensive equipment, reagents, and long readout time, thus making the process costly and difficult for onsite applications and causing a delay in the pathogen detection, preventing immediate medical action toward infected patients. There is a keen interest in developing new rapid point-of-care biosensing systems for early detection of pathogens with high sensitivity and specificity.

Recent developments in micro- and nanotechnology offer many technological advances in fabricating devices that incorporate nanoscale features to enhance sensitivity, reduce detection time, and enable multiplexing capability [9–12]. Most important, the properties of nanomaterials can be tailored by changing the size, shape, and composition, modifying the nanomaterial surface with appropriate functionalization, and conjugation with affinity ligands, antibodies, epitopes, and aptamers [13, 14]. Representative nanomaterials utilized for pathogen detection include metal nanoparticles [15–17], nanotubes and nanofibers [18], quantum dots [19], and magnetic nanoparticles [20]. These nanomaterials are used in conjugation with signal transduction techniques [21] such as fluorescence [22], bioluminescence [23], flow cytometry [24], colorimetry [25], electrochemistry [26–29], piezoelectrics [30], surface plasmon resonance (SPR) [31], quartz crystal microbalance [32], chemiluminescence [33], optical waveguides [34], and surface-enhanced Raman spectroscopy (SERS) [17, 25, 35–39].

In this chapter, we summarize an innovative pathogen capture and detection system based on dielectrophoresis (DEP). The device is a unique assembly of nanoelectrode arrays (NEAs) fabricated with vertically aligned carbon nanofibers (VACNFs) and a transparent macroscopic indium tin oxide (ITO) glass electrode in a "point-and-lid" geometry in which pathogens are

introduced using microfluidic channels. The study of capture kinetics was accomplished using fluorescence, SERS, and impedance measurement techniques. The test pathogens utilized in this study were bacteria such as *E. coli* DHα5 (nonpathogenic) and viruses such as bacteriophage and inactivated vaccinia virus. There have been several reports on using microscale DEP devices for manipulation of mammalian cells (tens of microns) to bacterial cells (~1.0 micron) [40]. The DEP force is proportional to the volume of the target particles [41] and decreases rapidly when the particle size is reduced to only ~100 nm. Therefore it becomes essential to fabricate nanostructured DEP electrodes to capture virus particles due to their small sizes (ranging from 10s nm to 300 nm). We illustrate in this chapter the method to use VACNFs for fabricating stable nanoscale DEP devices. The capture of virus *Bacteriophage* T4r and T1 using fluorescence and impedance sensing of vaccinia virus accompanied by electroporation has been accomplished due to the high electric field focused on the tips on VACNFs. Last, we have demonstrated the specific detection of bacterial cells using SERS reporter QSY21 that is co-functionalized with polyclonal antibodies on a special type of plasmonic nanoparticles, i.e., anisotropic oval-shaped iron-oxide-gold (IO-Au) core-shell nanoparticles. This dielectrophoretic device is integrated with a portable Raman system for rapid pathogen detection in field applications. Such integrated microfluidic systems provide simultaneous concentration and identification of specific microbes in dilute samples.

2. Principles, design, and fabrication

The phenomenon of dielectrophoresis (DEP) is renowned as a particle manipulation technique based on the uneven electrical force on the opposite sides of polarized particles in an electric field with a high gradient produced by the electrodes. The larger the electric field gradient, the stronger the DEP force acts on the particle. This phenomenon was first described by Pohl in 1951 [42] and has been widely used in biological science to separate live and dead bacteria [43, 44], viruses [45–47], cells [48–52], yeast cells [53, 54], and DNA [55–57]. When we consider radius of the particle r, the permittivity of the suspending medium ε_m, the gradient of the square of the applied electric field strength ∇E^2 and the real component of the complex Clausius-Mossotti (CM) factor $Re[K(\omega)]$, the time average DEP force (F_{DEP}) acting on the spherical particles by the nonuniform electric field, and the $Re[K(\omega)]$ are provided by the following equations:

$$\langle F_{DEP} \rangle = 2\pi r^3 \varepsilon_m \mathrm{Re}[K(\omega)]\nabla E^2, \tag{1}$$

where:

$$K(\omega) = \frac{\varepsilon_p^* - \varepsilon_m^*}{\varepsilon_p^* + 2\varepsilon_m^*}, \quad \text{where} \quad \varepsilon^* = \varepsilon - j\frac{\sigma}{\omega} \tag{2}$$

The use of physical fields for the separation of cells takes advantage of the heterogeneity of physical parameters for Eq. (2), such as ε^*, representing the complex permittivity and the indices p and m referring to the particle and medium, respectively; parameter σ is the conductivity; ω is the angular frequency ($\omega = 2\pi f$) of the applied electric field; and $j = \sqrt{-1}$. The direction of the force, either toward the field gradient as in positive DEP or away from it as in negative

DEP, is given by the difference in complex permittivity conductivity between the particle of interest and the suspending media. In this study, the proper medium (280 mM mannitol solution) is chosen to give $Re[K(\omega)] > 0$ so the particles experience a positive DEP (pDEP) force, directing toward higher electric field strength, which is desirable for capture bacteria and viruses at the exposed VACNF tips by selecting a proper frequency.

In the microfluidic device, a particle experiences two forces orthogonal to each other, i.e., DEP force (F_{DEP}) forcing the particles to capture on the tips and hydrodynamic force to carry the particles with the flow (i.e., Stokes drag force F_{Drag}) (as shown in **Figure 1d**). F_{DEP} is proportional to the volume or cube of the radius (r^3) of the particle. F_{Drag} is directly proportional to the radius of the particle by

$$F_{Drag} = 6\eta\pi r k \upsilon \tag{3}$$

where η is the dynamic viscosity, k is a small factor accounting for the wall effects, and υ is the linear flow rate (flow velocity). Sedimentation force and Brownian force are negligible for bacteria but not for submicron particles. The advantage of nanostructured DEP devices is that the magnitude of ∇E^2 can be enhanced by orders of magnitude so even small viral particles can be captured.

3. DEP device fabrication and setup for pathogenic particles

Figure 1a is the image of the device produced in the lab at Kansas State University. The detailed procedure of device fabrication is given in reference [58]. **Figure 1a** shows that the size of the devices is comparable to a US penny and illustrates the "points-and-lid" design. **Figure 1b** shows that the NEA comprises randomly distributed VACNFs (diameter ~100–120 nm, the density of ~2 × 10⁷ exposed CNFs/cm²) embedded in silicon dioxide (SiO_2) matrix (tip exposed) with an average spacing of ~1–2 μ. The active area exposed on NEA is 200 × 200 μm², and the rest is covered with a 2-μm-thick photoresist film to shield the effect of the rest of exposed tips. The ITO glass slide containing a photolithographically fabricated 500-μm-wide microfluidic channel in an 18-μm-thick photoresist film is permanently vacuum bonded.

In the experimental setup, DEP device was placed under an upright fluorescence optical microscope (Axioskop II, Carl Zeiss) using 50 X objective lens. The microorganisms such as *Bacteriophage* T4r (labeled with SYBR green I dye) and *E. coli* DHα5 (Alexa 555) fluorescence detection filter sets were configured to an excitation wavelength of 540–552 nm and an emission wavelength of 567–647 nm (filter set 20HE, Carl Zeiss). For vaccinia virus detection, filter sets were configured to 465–505 nm excitation wavelength and an emission wavelength of 515–565 nm (filter set 17, Carl Zeiss) for 3,3'-Dioctadecyloxacarbocyanine (DiO) dye and an excitation wavelength of 620–640 nm and an emission wavelength of 640–740 nm (filter set 60, Carl Zeiss) for propidium iodide (PI) dye. The videos were recorded using Axio Cam MRm digital camera to record fluorescence videos at varying exposure times depending on the pathogen species using multidimensional acquisition mode in the Axio-vision 4.7.1 release software (Carl Zeiss MicroImaging, Inc.). To prevent biofouling, the microfluidic channel was
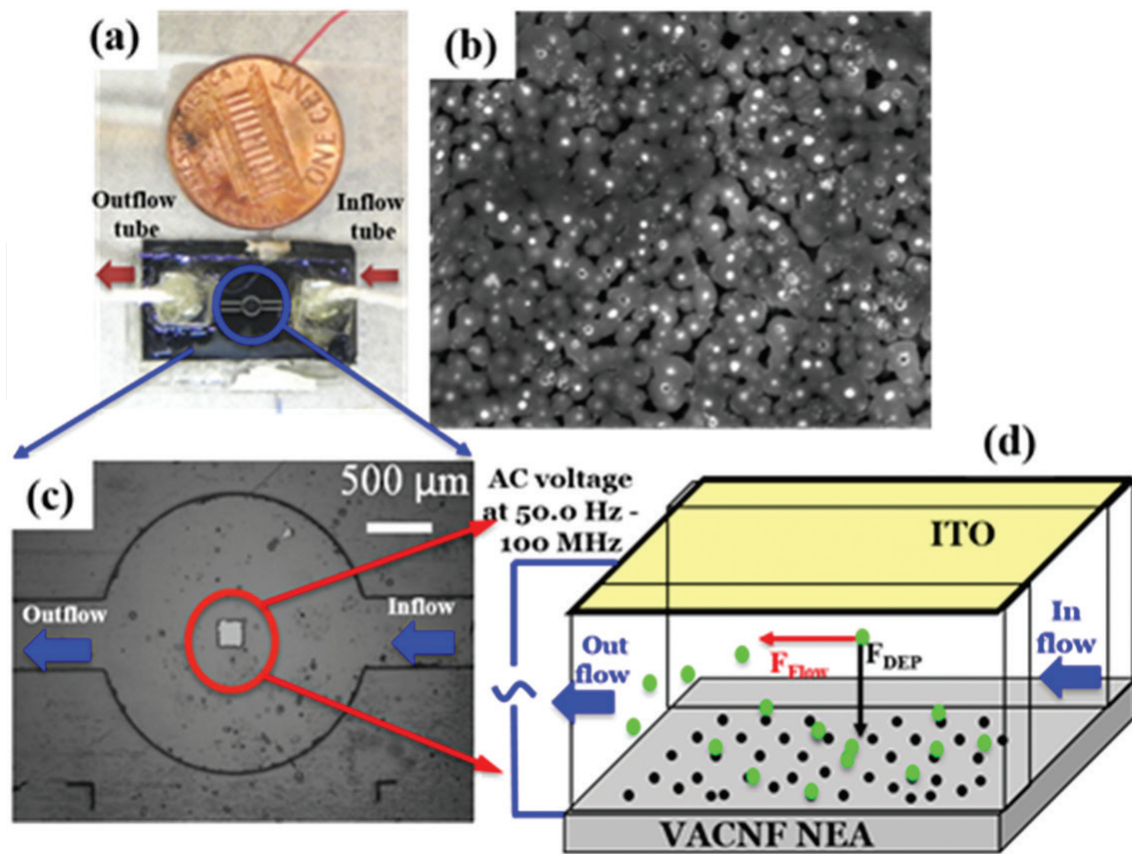
Figure 1. The embedded vertically aligned carbon nanofiber (VACNF) and indium tin oxide (ITO) DEP devices. (a) An example microfluidic device fabricated using indium tin oxide-coated glass and a nanoelectrode array chip covered exposing a 200 × 200 μm² area, glass fluidic connectors, and microbore tubes. (b) Scanning electron microscope (SEM) image of exposed tips (bright spots) of the VACNFs embedded in a silicon oxide layer. (c) A low-magnification optical microscope image showing the 200 × 200 μm² capture area. (d) Schematic diagram of microbial particles in the active nano-DEP area, which is subjected to the hydrodynamic drag force (F_{Drag}) along the flow direction and the dielectrophoretic force (F_{DEP}) perpendicular to the NEA surface. (Reprinted with permission from Madiyar et al. [59]; Foram Ranjeet et al. [61]).

injected with 1.0 mL bovine serum albumin (BSA) solution (2.0 gm in 100 mL of water) at a flow rate of 0.2 μl/min before performing DEP experiments. The channel was then rinsed with 2.0 mL DI water at a flow rate of 5.0 μl/min. **Figure 1c** shows the microfluidic design in which the particles entered from the narrow straight channel (500 μm in width) are distributed into the larger circular microchamber (2.0 mm in diameter), and only a fraction of the particles are passed over 200 × 200 μm active NEA area. Using this setup, bacteria *E. coli* DHα5 counting was accomplished using Axio software. In contrast, when detecting viral particles, it became difficult to distinguish the single viral particles. Hence for virus capture experiments, the integrated fluorescence intensity over the 200 × 200 μm active NEA area was recorded. For this, the initial fluorescence background (F_0) immediately before the V_{pp} was applied was subtracted from the final fluorescence signal (F_F) at the end of the capture period, giving the fluorescence intensity increase (ΔF) to represent the quantity of captured virus. The counts of isolated bright spots of single viral particles were observed at much lower virus concentration and were used in some later experiments to quantify the capture efficiency during the kinetic DEP process [59].

4. Detection of viruses: Bacteriophages and vaccinia virus using fluorescence and impedance method

4.1. DEP capture and kinetics of *Bacteriophage* T4r using fluorescence method

Bacteriophage T4r (Carolina Biological Supply Company, Burlington, NC) and T1 (ATCC, Manassas, VA) were utilized as probes to show the capability of the capture of nano-sized particles on VACNF tips. The culture of the *Bacteriophage* T4r using *E. coli B* is described in the previous report [59]. To label the virus particles, the virus solution was filtered through 0.2 μm filter (Fisher, PA) to remove the live bacteria or bacterial debris. To label the viruses, a 500 X working solution of SYBR® Green I Nucleic Acid Gel Stain (Lonza, Rockland, ME) in TE buffer (100 mM Tris [pH 7.6], 50 mM EDTA) was used, and the washing steps were accomplished using Amicon® Ultra 0.5 centrifugal filter devices (Millipore, Billerica, MA). The counting of viruses was carried out using double-layer agar technique after filtering the virus solution. The final wash was accomplished using 280 mM mannitol solution to enhance the efficiency of pDEP capture by manipulating the CM factor of viruses. The final concentration of the phages was ~5×10^9 pfu/mL except in some concentration-dependent experiments [59].

Figure 2 depicts the increase in an integrated fluorescence intensity to a saturation level in less than 10.0 s as a 10 V_{pp} AC bias when applied to the DEP device while flowing 5×10^9 pfu/mL *Bacteriophage* T4r solution through the channel at the flow velocity varying from 0.085 to 3.06 mm/s while changing the frequency from 100 Hz to 1.0 MHz. **Figure 2a** shows the maximum capture frequency to be 10 kHz. **Figure 2b**, a plot of the integrated fluorescence intensity of captured viruses vs. the flow velocity, showed a maximum at 0.73 mm/s. At $v \leq 0.73$ mm/s, isolated bright spots were seen (**Figure 2c**). At $v \geq 0.73$ mm/s, viruses depicted fractal-like lightening patterns (**Figure 2d**). These patterns are called *Lichtenberg figures*, which occur when the high electric field is produced at a sharp electrode surrounded by a relatively high concentration of polarizable particles. Previously such pattern was observed using *E. coli* cells between interdigitated microelectrodes called as "pearl-chain-like" Suehiro et al. [59, 62] This is first time that such pattern was observed with virus particles with the electric field produced at the nanoelectrode tips [59].

The DEP kinetics dramatically changed with concentration (**Figure 2e**) when two diluted concentrations, i.e., 5.5×10^8 and 2.5×10^7 pfu/ml, were used. The viruses could be individually counted (40 out of 67 particles) at an extremely low concentration of *Bacteriophage* T1 (8.7×10^4 pfu/mL) when passed through the nano-DEP device as the capture was limited by mass transport giving a capture efficiency ~60% [59].

4.2. DEP capture and electroporation of vaccinia virus coupled with real-time impedance detection

Electrochemical sensors based on impedimetric measurements have emerged as an attractive low-cost portable technique for the rapid detection of pathogenic microbes and other microorganisms. In this capture study, vaccinia virus was a probe to study the impedance kinetics and electroporation of the viruses due to high electrical field gradient generated at VACNFs tips.
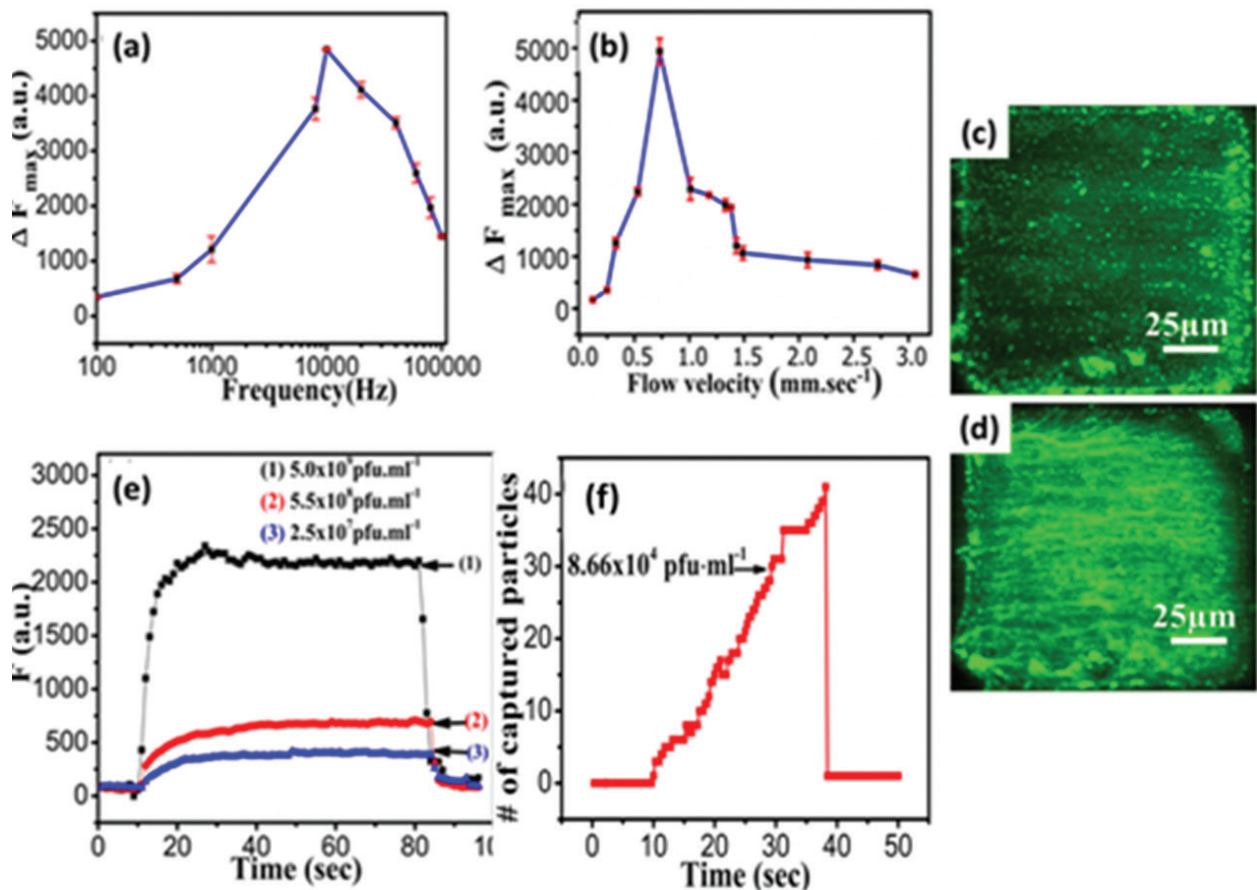
Figure 2. DEP capture of virus particles (*Bacteriophage* T4r) on VACNF in a microfluidic device. (a) The frequency dependence of DEP capture of 5×10^9 pfu/m *Bacteriophage* T4r at a flow velocity of 0.73 mm/s with the AC bias fixed at 10 V_{pp}. The optimum capture was obtained with ~10 kHz AC voltage by measuring integrated fluorescence intensity (ΔF_{max}). (b) The flow rate-dependent DEP capture peaked at 0.73 mm/s. (c) and (d) are the representative snapshots from the videos just before the AC voltage was turned off at a flow velocity of 0.33 and 0.73 mm/s, respectively. (e) The kinetic DEP capture curves at the standard concentration (5×10^9 pfu/ml) and two diluted concentrations (5.5×10^8 and 2.5×10^7 pfu/ml). (f) A kinetic profile of the *Bacteriophage* T1 capture at a low concentration at the flow velocity of 0.87 mm/s showing capture efficiency of 60%. (Reprinted with permission from Madiyar et al. [59]).

The details of the growth and enumeration by conventional techniques are given in a previous report [60]. Briefly, in-house stocks of vaccinia virus (*Copenhagen strain*, VC-2) were amplified by standard virus growth techniques of infecting HeLa cells knocked-down for an antiviral protein kinase, PKR (HeLa PKR-KD), followed by sucrose gradient centrifuge to achieve an optimal yield of 2.0×10^8 pfu/mL quantified via plaque assay. To move the viruses out of biosafety level 2 (BSL-2) containment, a UV-inactivation process was carried out by placing them 3–8 cm directly below a UV lamp (234 nm), and the plate was manually rocked for 10 min. The vaccinia viruses were dually labeled with 50 μM DiO lipophilic dye (Life Technologies, Carlsbad, CA) that stains the outer envelope of the virus by incubating the viruses at 37°C for 2 h. The washing of vaccinia virus was performed similarly as the bacteriophage virus. The concentration of the virus for the experiment was ~3×10^6 pfu/mL (except specified experiments). The nucleic acid (DNA) of the viruses was labeled with 50 μl 20.0 μM of propidium iodide (PI) aqueous solution. All the solutions were filtered with 0.2 μm filter and sterilized at 121°C for 20 min [61].

The details of the fluorescence experiment setup and videos are described in Section 3.0. The frequency (f), flow velocity (v), and concentration kinetic response of vaccinia virus cells were monitored using a fluorescence microscope. The experiments lasted for 85 s, during which no voltage (V_{off}) was applied in the first ~16 s, fixed AC voltage at different frequencies was applied (V_{on}) for ~54 s, and no voltage was applied (V_{off}) in the last ~15 s.

The integrated fluorescence intensity was measured at the end of capture period (54.0 s) and compared to the percentage change of the final impedance signal (Z_F) relative to the initial impedance signal (Z_o), i.e., %($Z_F - Z_o$)/Z_o. The optimum flow velocity for vaccinia virus was 0.40 mm/s at the frequency of 50.0 Hz and the voltage of 8.0 V_{pp} as shown in **Figure 3a**. The optical image is shown in **Figure 3c** which indicates the *Lichtenberg figures* (similar to *Bacteriophage* T4r) at the frequency of 50.0 Hz, but no capture was observed at 500 kHz (**Figure 3e**). Due to high biofouling of the vaccinia virus at the frequency 50.0 Hz, the frequency of 1.0 kHz (**Figure 3d**)
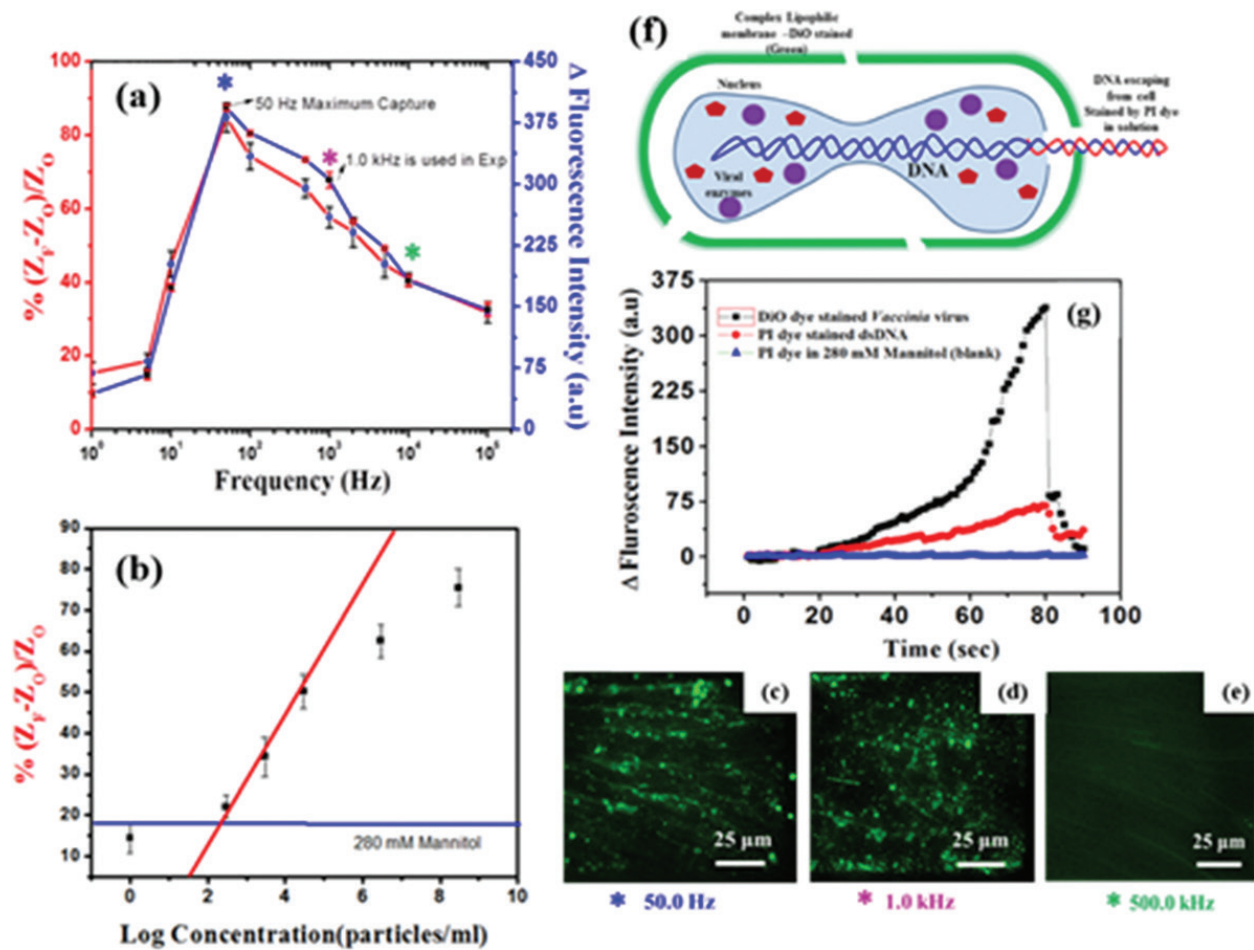

Figure 3. Assessing DEP capture and electroporation of vaccinia virus particles. (a) The frequency dependence of DEP capture ranging from 10.0 Hz to 1.0 MHz at fixed flow velocity (0.40 mm/s) and fixed AC voltage (8.0 V_{PP}) peaking at 50.0 Hz. (b) The calibration curve of the percentage change in the impedance after 54 s DEP versus the logarithm of the virus concentration ranging from 3.0×10^2 to 3.0×10^6 pfu/ml. (c–e) Snapshots from the fluorescence video after 54 s of DEP capture of vaccinia virus at a fixed flow velocity of 0.401 mm/s at various AC frequency of (c) **50.0 Hz,** (d) **1.0 kHz,** and (e) **10 kHz**. (f) The schematic image of electroporation of vaccinia virus particles in which the vaccinia viruses are dually stained using DiO dye for outer lipophilic membrane (green) and propidium iodide (red) for dsDNA (inside or extracted out of the vaccinia virus). (g) The increase in the fluorescence signal of the DiO and PI dye during DEP capture of vaccinia virus and the PI dye mixed in 280 mM mannitol solution as the control experiment. (Reprinted with permission from Madiyar et al. [69]).

was used as the capture frequency (except few experiments). A concentration $\sim 3 \times 10^3$ to 3×10^6 pfu/mL was employed to demonstrate concentration-dependent study with the real-time potential and measures the limit of detection of the impedance method. For this experiment, the frequency is fixed at 1.0 kHz, and the 0.5 V_{PP} AC voltage is applied for 16 s to obtain the background impedance value. The AC voltage is then increased to 8.0 V_{PP} for 54 s to capture the virus (indicated by the increase in the impedance signal). The AC voltage is finally reduced back to 0.5 V_{PP}, indicating the release of the virus particles from the VACNF tips. The control experiment is done under the same conditions using blank 280 mM mannitol solution. The calibration curve (**Figure 3b**) shows that the logarithm of virus concentration (C) in the range from ~300 to 30,000 particles/mL is linear with percentage impedance change collected over the 200 × 200 μm active area. Using the calibration curve equation (details in Refs. [61, 66]), the detection limit of vaccinia virus was calculated to be ~ 300 particles/mL [61].

Finally, to investigate the electroporation of lipophilic membrane due to the high electric field on tips of VACNF NEAs, PI dye was added to the mannitol solution containing 3.0×10^6 particles/mL of DiO dye-labeled vaccinia virus and observed in Neubauer chamber. The absence of the red fluorescence indicated there was no structural damage of virus due to UV inactivation [62]. For electroporation experiment in a microfluidic device, the frequency of 50.0 Hz was used. The voltage of 8.0 V_{PP} was turned on for 65 s for maximal DEP capture with the flow velocity set at 0.05 mm/s (for maximum capture and interaction of dye and DNA). **Figure 3f** shows the schematic figure of electroporation of lipophilic membrane of vaccinia virus in the presence of high electric field at the VACNF tips. It is observed that the electroporation made the membrane more permeable and the DNA is likely extracted out of the membrane to interact with PI dye in the mannitol solution which increases the PI dye fluorescence intensity. There is evidence that, after the AC voltage is turned off, some PI-intercalated ds-DNAs are physically adsorbed on the VACNF tip or the NEA chip surface [61, 63].

5. Detection of bacteria: DEP capture and identification of *E. coli* strain DHα5 by surface-enhanced Raman spectroscopy

DEP capture of bacterial cells was demonstrated with nontoxic *E. coli* strain DHα5 (18265-017, Fisher Scientific). The DEP microfluidic device with Raman setup is schematically represented in **Figure 4a**. The procedure for fluorescent labeling and attachment of the bacteria with a unique SERS nanotag consisting of nanooval (NOV)-shaped gold coating on spherical iron-oxide (IO) nanoparticles is reported in Ref. [62]. Gold is coated on the spherical IO nanoparticle cores (~23 nm diameter), forms an outer dimension of ~50 nm with NOVs which demonstrates high SERS enhancement factor due to Raman tag of QSY-21. The NOVs are made biocompatible, and surface active by adding carboxylic acid groups at the surface was accomplished by coating them with carboxyl-polyethylene glycol-thiol (HOOC-PEG-SH, MW 5000) and methoxy-polyethylene glycol-thiol (mPEG-SH, MW 5000). The details of the process are given in Ref. [63, 66]. The carboxylic acid group aids in the formation of amide covalent bonds with secondary IgG antibody conjugated with Alexa 555 making the IO-NOVs fluorescently labeled. These secondary antibodies are complementary to IgG antibody conjugated
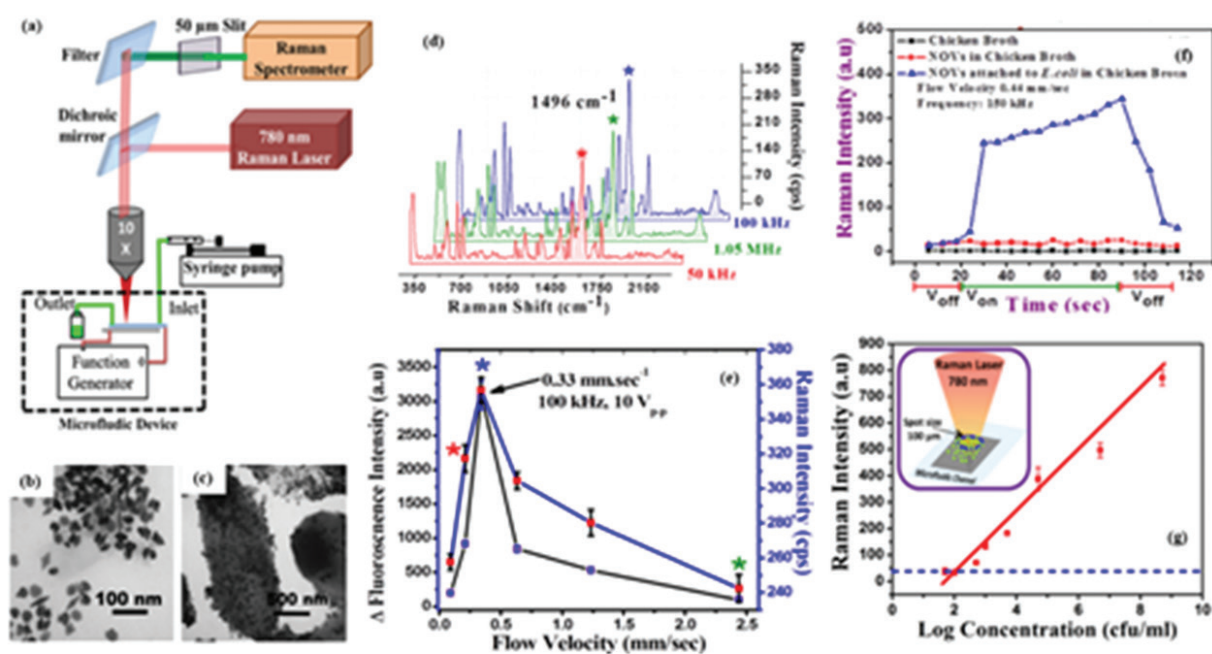
Figure 4. Capture of *E. coli* Dhα5 in NEA microfluidic channel. (a) Schematic of the microfluidic dielectrophoretic device under a Raman microscope for bacteria detection. TEM images of (b) the starting IO-Au NOVs and (c) *E. coli* DHα5 bacterial cells attached with antibody-functionalized IO-Au NOVs. (d) Assessing DEP capture of 5.3 × 10⁵ CFU/mL *E. coli* cells with fluorescence and Raman measurements at varying frequency with the fixed voltage at 10.0 V$_{PP}$ showing 1496 cm⁻¹ is the highest peak. (e) The study of *E. coli* cells at varying flow velocity at a fixed frequency (100 kHz) and voltage (10 V$_{PP}$). (f) The study of DEP capture of *E. coli* cells with Raman measurements in different complex matrices such as chicken broth. The DEP capture kinetics using a chicken solution were performed at 10.0 V$_{PP}$, 0.44 mm/s flow velocity, and 150 kHz AC frequency. (g) The calibration curve plotted with the concentration varying from 5 CFU/mL to 1.0 × 10⁹ CFU/mL (X-axis) and the Raman intensity after 50 s of DEP capture (Y-axis). The Raman intensity measurements with a ProRaman L portable Raman system (Enwave Optronics) with laser focal spot of 100 μm diameter aligned with active DEP area (inset). (Reprinted with permission from Madiyar [66]).

with FITC primary antibody which was attached to bacteria *E. coli* DHα5. The detailed procedure is given in reference [63, 64]. **Figure 4b** and **c** show TEM images of IO-Au SERS NOVs and those bound to *E. coli*. The typical Raman spectrum of QSY21 has prominent bands at 1333, 1584, and 1641 cm⁻¹ which are from the xanthene ring stretching vibrations of the molecule [65]. The intensity of QSY21 marker at the Raman shift of 1496 cm⁻¹ is visually separated from the carbon nanofiber signals at 1350 cm⁻¹ (D-band) and 1600 cm⁻¹ (G-band), respectively [66]. The most reliable characteristic band is seen at 1496 cm⁻¹ as seen in **Figure 4d** was used to quantify the SERS signal.

To demonstrate the potential of this method, both confocal (DXR, Thermo Fisher Scientific) and portable systems (ProRaman L, Enwave Optronics. Inc) were used. The similar studies were carried out with the two spectrophotometers at varied flow velocity and frequency. **Figure 4d** shows the full Raman spectrum of QSY21 at different AC frequencies during the capture of bacteria. The highest peak in the full spectra, 1496 cm⁻¹, was used in the further calculation, and the higher capture was seen at the AC frequency of 100.0 kHz. The results between these two Raman systems were very consistent from their fluorescence and Raman intensity plots, with the maximum flow velocity at 0.4 mm/s (0.55 μl/s) (**Figure 4e**).

To analyze the capture in complex samples, one of the representative data is shown in **Figure 4f**, i.e., the capture of *E. coli* in the chicken broth samples. Other samples such as Mott's apple juice and soil samples were also tested, and details are given in Ref. [62]. Complex matrix solution was centrifuged at 14,000 rpm for 10 min, and the supernatant was collected. Complex matrices present different challenges due to inorganic and organic substance interactions, making it difficult to isolate the target to be tested. A concentration of 5×10^5 cells/mL *E. coli* DHα5 was added into the solution of processed chicken broth [66]. The conductivity of bacteria in distilled water (pH 6.8) was 1.22×10^{-4} S/m. The conductivity of commercial chicken broth after sample processing and adding *E. coli* DHα5 cells resulted in conductivity of 1.7×10^{-3} S/m. Due to the change in solution (chicken broth) conductivity, the bacteria in complex matrices have a high Raman intensity at the frequency of 150.0 kHz and for soil solution 100.0 kHz.

Figure 4g summarizes the SERS intensity of the captured NOV-labeled *E. coli* using the portable Raman setup, while the *E. coli* concentration was varied from ~10 to 1×10^9 cells/mL. The probe diameter at the focal point in the portable Raman system is about 100 µm (inset in **Figure 4g**), much larger than the 3.1 µm size in the confocal Raman microscope allowing signals to be collected from many more bacteria, and yields better statistics of the detection limit measurement [66]. The calibration curve for the detection limit measure is shown in **Figure 4g**. The Raman intensity was a linear function of the logarithm of bacteria concentration when the concentration C is above ~100 cells/mL [66]:

$$(RI)_{portable} = 108.8 \times \log C - 214.7 \qquad (4)$$

where RI was the Raman intensity increase after 50 s of DEP capture. For bacteria concentrations below the critical value, $C_0 = $ ~100 cells/mL. There was no measurable signal detected above the background, i.e., $(RI)_{blank} = $ ~36 a.u. Due to the slow mass transport of bacteria to the active area, no captured bacterial cells were detected during the applied DEP period. However, at the time when the high concentration of the bacteria was passed, the Raman intensity increased. The detection limit $\log C_{dl}$ was determined using calibration curve:

$$\log C_{dl} = \log C_0 + 3\, s_{blank}/m, \qquad (5)$$

where s_{blank} (~11.7) is the standard deviation of the Raman signal for bacteria concentration below C_0 and $m = 108.8$ is the slope of the calibration curve. The concentration detection limit was determined to be ~210 cells/mL.

6. Discussion and conclusion

The physical phenomenon of DEP was observed on the tips of VACNF NEAs in microfluidic channel design due to high electric field gradient generated by the "point-and-lid" geometry acted as an effective and reversible electronic manipulation technique to rapidly (less than 60 s) concentrate bacteria and viruses into a micro-area from the solution flow. The nanoscale size of the VACNF tips has two critical features: the extremely high electrical field strength

at the tip (E = ~10^7 V m^{-1}) and the large electric field gradient at the tips of nanoelectrode (giving $\nabla E^2 = 10^{19} - 10^{20}$ V^2 m^{-3}) against ITO electrode. The polarizable pathogenic particles in the microfluidic device encounter hydrodynamic drag force along the flow direction and orthogonal (vertical) DEP forces due to the high electric field gradient. Once the pathogens are close to the VACNF tip, the lateral DEP force becomes larger than the hydrodynamic drag force, and the pathogens are captured at the nanoelectrode tip.

According to Eq. (1), the force of DEP highly depends on the volume of the particles (r^3) and the optimal frequency for capture bacteria, *E. coli*, *Bacteriophage* T4r, and vaccinia virus at the NEA tips was found to be 100 kHz, 10.0 kHz, and 50 Hz, respectively. This variation is due to the differences in size, structure, and molecular composition. *Bacteriophage* T4r virus has ~ 80–100 nm icosahedral-shaped protein capsid encapsulating ds-DNAs [67]. Vaccinia virus particles are larger spheres with dimensions of 360 × 270 × 250 nm, which consist of the lipophilic membranes encapsulating ds-DNAs [68]. Bacteria *E. coli* DHα5 is ~1 micron with an elongated shape and more complex internal structures [69, 70].

The second drastic contrast in the capture of viruses is the formation of *Lichtenburg figures* which was absent during capture of the bacteria. This is due to the spatial distribution of the electrical field strength at the nanoelectrode tip. *Bacteriophage* T4r and vaccinia virus are similar in size and are comparable to the diameter of VACNFs, causing the viruses to be polarized to a large extent. The captured virus acts as an extended tip attracting more viruses toward it. For bacteria, the more significant size (~1 μ) and higher internal conductivity may have screened the high electric field at the nanoelectrode tip and reduced the electrical interaction with additional cells [58, 59, 64, 70].

The device successfully captured single virus particles observed at isolated spots in the 200 × 200 μm^2 active NEA surface at an extremely dilute concentration (8.9 × 10^4 pfu/ml) in which facilitated studying the impedance kinetics of real-time DEP capture of vaccinia viral particles, yielding a detection limit of 300 particles/ml. VACNF tips have been found to cause electroporation of the lipophilic membrane of the vaccinia virus due to the large electric field produced on the tips. This electroporation phenomenon has allowed extracting the internal nucleic acid contents to the solution.

Finally, highly sensitive detection of *E. coli* bacteria using the SERS nanotag based on QSY21 on IO-Au NOVs proved to be highly sensitive. This was accomplished using two complementary antibodies, in which the secondary antibody was bonded to nanoovals and other to the bacteria. The attachment of the nanoovals significantly enhanced Raman signals and aided in specific recognition to *E. coli* DHα5 cell. The detection and kinetics of capture were studied using both a confocal Raman microscope and a portable Raman system, and the limit of detection of 210 CFU/mL was calculated by calibration curve using the portable Raman system.

All these studies revealed the exciting interplay between the highly focused electric fields at the nanoelectrode with bioparticles of comparable sizes. The device was successfully integrated with fluorescence, surface-enhanced Raman spectroscopy and electrochemical impedance sensing. All these results are very encouraging and can be further improved by optimizing the DEP design. The combined functions of DEP in concentration, detection, and electroporation make such nano-DEP devices useful to extract intracellular materials, such as DNA or proteins

without a lytic agent. It can act as an on-chip portable sample preparation module for potentially capturing pathogenic particles at concentrations approaching 1–10 particles/mL and for future downstream processing and testing of microbial samples.

Author details

Foram Ranjeet Madiyar[1,2]*, Omer Farooq[2] and Jun Li[1]

*Address all correspondence to: madiyarf@erau.edu

1 Department of Chemistry, Kansas State University, Manhattan, KS, United States

2 Department of Physical Sciences, Embry Riddle Aeronautical University, Daytona Beach, FL, United States

References

[1] WHO news release World Health Organization. 2015

[2] Law JW-F, Ab Mutalib N-S, Chan K-G, Lee L-H. Frontiers in Microbiology. 2014;**5**:770

[3] Ivnitski D, Abdel-Hamid I, Atanasov P, Wilkins E. Biosensors and Bioelectronics. 1999; **14**:599-624

[4] Lazcka O, Campo FJD, Muñoz FX. Biosensors & Bioelectronics. 2007;**22**

[5] Espy MJ, Uhl JR, Sloan LM, Buckwalter SP, Jones MF, Vetter EA, Yao JD, Wengenack NL, Rosenblatt JE, Cockerill FR, Smith TF., Clinical Microbiology Reviews. 2006;**19**:165-256

[6] Mackay IM. Clinical Microbiology and Infection. 2004;**10**:190-212

[7] Fung DYC. Food Reviews International. 1994;**10**:357-375

[8] Ahmed A, Rushworth JV, Hirst NA, Millner PA. Clinical Microbiology Reviews. 2014; **27**:631-646

[9] Mairhofer J, Roppert K, Ertl P. Sensors. 2009;**9**:4804

[10] Heo J, Hua SZ. Sensors. 2009;**9**:4483

[11] Khoshmanesh K, Nahavandi S, Baratchi S, Mitchell A, Kalantar-zadeh K. Microfluidics and Nanofluidics. 2011;**26**

[12] Leonard P, Hearty S, Brennan J, Dunne L, Quinn J, Chakraborty T, O'Kennedy R. Enzyme and Microbial Technology. 2003;**32**

[13] Byrne B, Stack E, Gilmartin N, O'Kennedy R. Sensors. 2009;**9**:4407

[14] Sharma S, Byrne H, O'Kennedy RJ, Essays in Biochemistry. 2016;**60**:9-18

[15] Tu S-I, Reed S, Gehring A, He Y, Paoli G. Sensors. 2009;**9**:717

[16] Sun H, Choy TS, Zhu DR, Yam WC, Fung YS. Biosensors & Bioelectronics. 2009;**24**

[17] Wang C, Madiyar F, Yu C, Li J. Journal of Biological Engineering. 2017;**11**:9

[18] Thuy NT, Tam PD, Tuan MA, Le A-T, Tam LT, Van Thu V, Van Hieu N, Chien ND. Current Applied Physics. 2012;**12**:1553-1560

[19] Liandris E, Gazouli M, Andreadou M, Sechi LA, Rosu V, Ikonomopoulos J. PLoS One. 2011; **6**:e20026

[20] Fauss EK, MacCuspie RI, Oyanedel-Craver V, Smith JA, Swami NS. Colloids and Surfaces B: Biointerfaces. 2014;**113**:77-84

[21] Sethi RS. Biosensors and Bioelectronics. 1994;**9**:243-264

[22] Lu Z, Zhang J, Xu L, Li Y, Chen S, Ye Z, Wang J. Sensors (Basel, Switzerland). 2017;**17**:442

[23] Baker JM, Griffiths MW, Collins-Thompson DL. Journal of Food Protection. 1992;**55**:62-70

[24] Rajwa B, Dundar MM, Akova F, Bettasso A, Patsekin V, Hirleman ED, Bhunia AK, Robinson JP. Cytometry. Part A: The journal of the International Society for Analytical Cytology. 2010;**77**:1103-1112

[25] Vidic J, Manzano M, Chang C-M, Jaffrezic-Renault N. Veterinary Research. 2017;**48**:11

[26] Pedrero M, Campuzano S, Pingarrón J. Sensors. 2009;**9**:5503

[27] DeSilva MS, Zhang Y, Hesketh PJ, Maclay GJ, Gendel SM, Stetter JR. Biosensors and Bioelectronics. 1995;**10**:675-682

[28] Ghindilis AL, Atanasov P, Wilkins M, Wilkins E. Biosensors and Bioelectronics. 1998;**13**: 113-131

[29] Ivnitski D, Wolf T, Solomon B, Fleminger G, Rishpon J. Bioelectrochemistry and Bio-energetics. 1998;**45**:27-32

[30] Prusak-Sochaczewski E, Luong JHT, Guilbault GG. Enzyme and Microbial Technology. 1990;**12**:173-177

[31] Liu Y, Liu Q, Chen S, Cheng F, Wang H, Peng W. 2015;**5**:12864

[32] Carter RM, Mekalanos JJ, Jacobs MB, Lubrano GJ, Guilbault GG. Journal of Immunological Methods. 1995;**187**:121-125

[33] Ramanathan S, Shi W, Rosen BP, Daunert S. Analytica Chimica Acta. 1998;**369**:189-195

[34] Mukundan H, Anderson A, Grace WK, Grace K, Hartman N, Martinez J, Swanson B. Sensors. 2009;**9**:5783

[35] Lazcka O, Campo FJD, Muñoz FX. Biosensors and Bioelectronics. 2007;**22**:1205-1217

[36] Singh R, Mukherjee MD, Sumana G, Gupta RK, Sood S, Malhotra BD. Sensors and Actuators B: Chemical. 2014;**197**:385-404

[37] Stöckel S, Kirchhoff J, Neugebauer U, Rösch P, Popp J. Journal of Raman Specroscopy. 2016;**47**

[38] Wu X, Xu C, Tripp RA, Huang Y-w, Zhao Y. Analyst. 2013;**138**

[39] Yang D, Zhou H, Haisch C, Niessner R, Ying Y. Talanta. 2016;**146**

[40] Toner M, Irimia D. Annual Review of Biomedical Engineering. 2005;**7**:77-103

[41] Wood NR, Wolsiefer AI, Cohn RW, Williams SJ. Electrophoresis. 2013;**34**:NA-NA

[42] Pohl HA. Journal of Applied Physics. 1951;**22**:869-871

[43] Lapizco-Encinas BH, Simmons BA, Cummings EB, Fintschenko Y. Analytical Chemistry. 2004;**76**:1571-1579

[44] Fernandez RE, Rohani A, Farmehini V, Swami NS. Analytica Chimica Acta. 2017;**966**:11-33

[45] Masuda T, Maruyama H, Honda A, Arai F. PLoS One. 2014;**9**:e94083

[46] Hughes MP, Morgan H, Rixon FJ, Burt JPH, Pethig R. Biochimica et Biophysica Acta (BBA) - General Subjects. 1998;**1425**:119-126

[47] Ermolina I, Milner J, Morgan H. Electrophoresis. 2006;**27**:3939-3948

[48] Gascoyne PRC, Ying H, Pethig R, Vykoukal J, Becker FF. Measurement Science and Technology. 1992;**3**:439

[49] Markx GH, Pethig R. Biotechnology and Bioengineering. 1995;**45**:337-343

[50] Becker FF, Wang XB, Huang Y, Pethig R, Vykoukal J, Gascoyne PR. Proceedings of the National Academy of Sciences. 1995;**92**:860-864

[51] Pethig R, Menachery A, Pells S, De Sousa P. Journal of Biomedicine and Biotechnology. 2010;**2010**:182581

[52] Voldman J. Annual Review of Biomedical Engineering. 2006;**8**:425-454

[53] Huang Y, Holzel R, Pethig R, Xiao BW. Physics in Medicine & Biology. 1992;**37**:1499

[54] Markx GH, Talary MS, Pethig R. Journal of Biotechnology. 1994;**32**:29-37

[55] Pethig R. Biomicrofluidics. 2010;**4**:022811

[56] Gascoyne PRC, Vykoukal J. Electrophoresis. 2002;**23**:1973-1983

[57] Asbury CL, Diercks AH, van den Engh G. Electrophoresis. 2002;**23**:2658-2666

[58] Syed LU, Liu J, Price A, Li Y-f, Culbertson C, Li J. Electrophoresis. 2011;**32**:2358-2365

[59] Madiyar FR, Syed LU, Culbertson CT, Li J. Electrophoresis. 2013;**34**:1123-1130

[60] In: Jones TB. ed, Electromechanics of Particles. Cambridge: Cambridge University Press; 1995. pp. 139-180

[61] Madiyar FR, Syed LU, Arumugam P, Li J. Advances in applied nanotechnology for agriculture. American Chemical Society. 2013:109-124

[62] Junya S, Ryuichi Y, Ryo H, Masanori H. Journal of Physics D: Applied Physics. 1999; **32**:2814

[63] Bhana S, Rai BK, Mishra SR, Wang Y, Huang X. Nanoscale. 2012;**4**:4939-4942

[64] Arumugam PU, Chen H, Cassell AM, Li J. The Journal of Physical Chemistry A. 2007; **111**:12772-12777

[65] Huang X, Bhana S. Google Patents; 2015

[66] Madiyar FR, Bhana S, Swisher LZ, Culbertson CT, Huang X, Li J. Nanoscale. 2015;**7**:3726-3736

[67] Prasad BVV, Schmid MF. Advances in Experimental Medicine and Biology. 2012;**726**:17-47

[68] Griffiths G, Wepf R, Wendt T, Locker JK, Cyrklaff M, Roos N. Journal of Virology. 2001; **75**:11034-11055

[69] Madiyar FR, Haller SL, Farooq O, Rothenburg S, Culbertson C, Li J. Electrophoresis. 2017; **38**:1515-1525

[70] Li J, Madiyar FR, Swisher L. Carbon Nanomaterials for Biomedical Applications. In: Zhang M, Naik RR, Dai L, editors. Cham: Springer International Publishing 2016. pp. 113-143